BNL-NUREG-35520

CONF-8410208--1

Mechanisms of Stress Corrosion Cracking and Intergranular Attack in Alloy 600 in High Temperature Caustic and Pure Water

R. Bandy and D. van Rooyen

Brookhaven National Laboratory
Upton, NY 11973

BNL-NUREG--35520

TI85 005129

IN RECENT YEARS, several studies have been conducted on the intergranular stress corrosion cracking (SCC) and intergranular attack (IGA) of Alloy 600 (1-6). A combination of SCC and IGA has been observed in Allooy 600 tubing on the hot leg of some operating steam generators in pressurized water reactor (PWR) nuclear power plants, and sodium hydroxide along with several other chemical species have been implicated in the tube degradations (1,2). SCC has been observed above and within the tube sheet, whereas IGA is generally localized within the tube sheet (1,2). Alloy 600 is also susceptible to SCC in pure and primary water (3,4). Various factors that influence SCC and IGA include metallurgical conditions of the alloy, concentrations of alkaline species, impurity content of the environment, temperature and stress (1-6). The mechanisms of these intergranular failures, however, are not well understood. Some of the possible mechanisms of the SCC and IGA in high temperature water and caustic are described in this paper.

EXPERIMENTAL

In deaerated pure and primary water, the work involved U-bends, slow strain rate tests and C-rings. The primary water contained 10^{-4} M LiOH and 650 ppm of boron as boric acid with an H_2 overpressure of 0.1 MPa. The details of autoclave testing in pure and primary water, specimen preparation, materials and their composition have been published elsewhere (3,4).

In the caustic environments, our investigation was conducted using C-ring and straining electrode specimens. For C-rings, a nuclear grade Alloy 600 tubing, 19.1 mm OD and 1.07 mm wall thickness and the following composition by weight was used: 0.02 C, 0.23 Mn, 9.40 Fe, 0.001 S, 0.14 Si, 0.30 Cu, 74.27 Ni, 15.64 Cr, 0.24 Al, 0.31 Ti, 0.04 Co, 0.011 P, 0.005 B. The materials were mainly used in their mill annealed (MA) conditions. A few C-ring specimens were tested in the solution annealed (SA) and solution annealed plus sensitized (SAS) condition. SA samples were heat treated at 1050 C for 10 min. and rapidly air cooled. SAS samples were heated at 1100 C for 10 min. and water quenched before sensitization at 621 C for 18 h. Heating was in sealed tubes with an inert atmosphere. The C-rings were stressed on their OD in the usual way (7). The MA material was stressed at a maximum stress at the apex of the ring corresponding to 150% of the yield strength. The same deformation as for the MA material was applied on the SA and SAS C-rings. The solutions were prepared from distilled demineralized water of conductance less than 0.5 μ S and reagent grade NaOH pellets. In some cases, controlled amounts of sodium carbonate and sodium sulfate were added as impurities. All tests were conducted in the 300-315 C range for generally about 10 to 12 days. The static potential band method (8) used to control the potentials of the specimen(s) consisted, in the case of the C-rings, of passing a large current from a power supply through a string of samples sep rated from one another by known electrical resistors (platinum wires) while holding one of them at a fixed potential with a potentiostat. An iR drop was thus established between each sample of the series causing each one to attain a different electrochemical potential. Alloy 600 leads were spot welded to various C-rings to monitor their potentials. Figure 1 shows a schematic circuitry used for the multiple specimen studies. The reference electrode was made of nickel and the nickel autocalve body acted as the counter electrode. Before raising the temperature, the autoclave was deaerated by pressurizing to 3.45 MPa (500 psi) with nitrogen followed by a slow depressurization, the procedure being repeated five times. A 1.38 MPa overpressure of 5% hydrogen -95% nitrogen was then added. When a stable corrosion potential was established at the test temperature, the potentiostat and power supply were switched on.

A set of C-rings made from the Alloy 600 tubing of the above-mentioned composition was tested in the primary water in a Hastelloy C-276 autocalve using the electrical circuitry de-

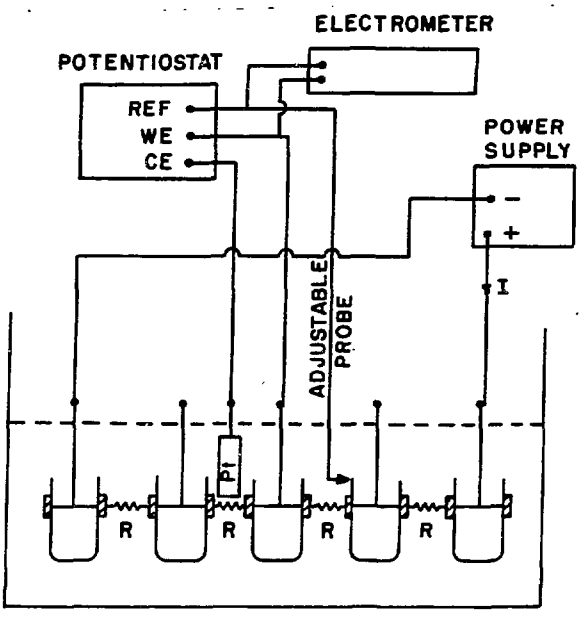

Fig. 1 - Schematic of circuitry for testing multiple specimens under potential control using the modified Seys and Van Haute Technique.

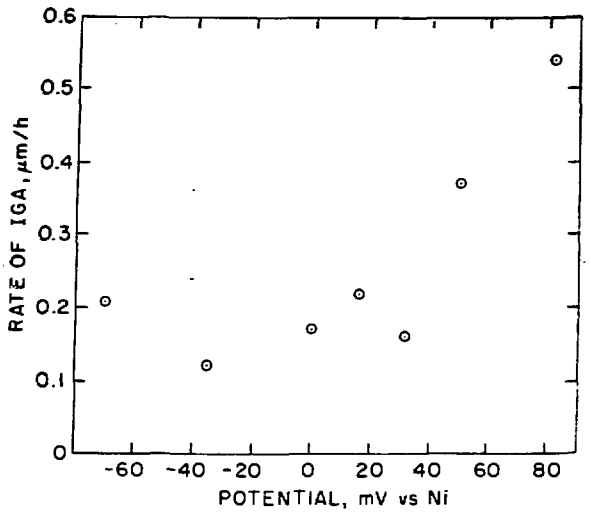

Fig. 3 - Relationsnip between electrochemical potential and average rate of IGA in mill-annealed (MA) C-rings in 10% NaOH + 0.1% Na_2CO_3 solution at 300 C. Test duration 343 hours.

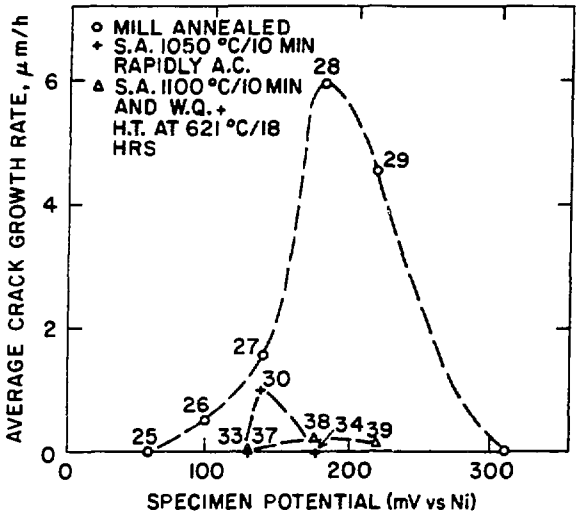

Fig. 2 - Potential dependence of average crack propagation rate of C-rings under three different metallurgical conditions in 10% NaOH + 0.1% Na_2CO_3 solution at 300 C. Numbers on figure refer to specimen nos.; test duration 168 hours.

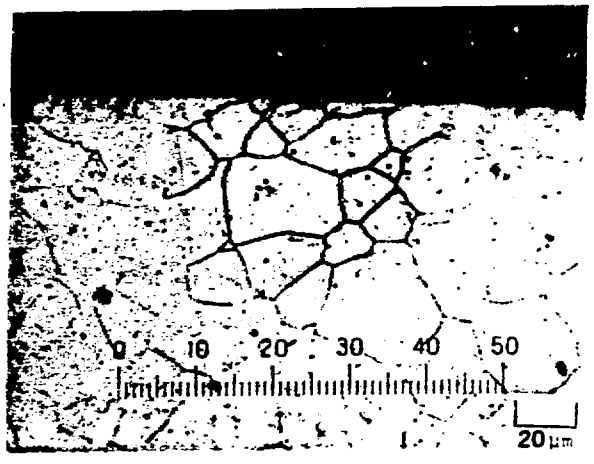

Fig. 4 - Typical IGA at +16 mV (vs. Ni) on a C-ring in Fig. 3.

scribed above. In this case, a platinum wire was used as the reference electrode.

The straining electrode test was conducted under potentiostatic control following procedures described elsewhere (9). Prior to straining, the desired potential was applied to the 1 mm diameter wire specimen and the current was allowed to reach a steady value. The specimen was then rapidly strained uniaxially at a rate of about 1% per second into the plastic region. The current transient thus caused was recorded, and used to calculate the crack propagation rate (CPR).

In another set of experiments, Alloy 600 coupons (12.5 mm x 25 mm) were exposed to the same environment and potentials as the C-rings. The coupons were polished with diamond paste to 1 μm finish. After withdrawal from the environment, the surfaces were examined under scanning electron microscope.

Potentiodynamic polarization was conducted using a PAR Model 173 potentiostat and Hewlett Packard Model 7047 X-Y recorder. An Elscint Model ABA-26 automatic Baseline Advance was used to obtain the desired scan rate.

RESULTS AND DISCUSSION

C-RING IN CAUSTIC - The potential dependence of the crack propagation rate of C-rings, tested by the modified Seys and Van Haute technique (8), in 10% NaOH + 0.1% Na_2CO_3 solution at 300 C is shown in Fig. 2. The CPR shown is the average value based on the total testing time and the maximum crack depth. The specimens were tested under MA, SA, and SAS conditions as described on the figure. The MA C-rings suffered rapid SCC between 100 and 220 mV in this test. Similar potential dependence of SCC of Alloy 600 in the caustic environment was observed by various previous investigators (5,6), and the excellent agreement between our results and those of the previous investigators provide good confidence in the technique employed by us. This technique with multiple C-rings proved to be a very useful one, leading to considerable saving in testing time and eliminating variations that can occur between individual tests. In their original method, Seys and Van Haute (8) used a wire specimen which itself acted like a resistor providing potential drop along its length. But they did not have any provision for precise potential measurement. In our modified method, since the specimens are separate with individual platinum wire leads, potential monitoring of each specimen can be easily performed. The method has recently been used successfully to study SCC at room temperature (10).

Fig. 2 shows that the crack propagation of the MA material is much higher than that of the SA or the SAS materials. However, because of the heat treatment, the SA and SAS materials have much lower yield strength, and since all our C-rings were given the same amount of deflection, the stress level reached by the SA and SAS C-rings were lower than that of the MA C-rings. Therefore, it is not clear whether this factor is responsible for an apparent improvement in SCC performance or whether the heat treatments actually improved SCC resistance. In the literature, there is ample evidence that sensitizing heat treatments generally improve the caustic SCC resistance of Alloy 600 (5,6). However, one study (11) shows that U-bends of SAS Alloy 600 (1120 C, 1 h, WQ + 675 C, 2 h) generally registered greater crack growth in deaerated 50% NaOH at 315 C in 5 weeks than U-bends of the SA material (1120 C, 1 h, WQ). The mechanical properties and the grain size were very similar in the above two thermal conditions.

In some potential regions, specimens suffered IGA instead of any sharp crack. Fig. 3 shows the relationship between specimen potential and the rate of IGA in 10% NaOH + 0.1% Na_2CO_3 solution at 300 C. The rate is an average value calculated by dividing the maximum ICA depth observed on any specimen by the total testing time. A typical IGA on a sample held at about +16 mV is illustrated in Fig. 4. It appears that the rate of attack generally increases with increasing anodic potential, and the material is also susceptible to IGA in the cathodic region. At present we do not have enough data to establish the relationship between IGA rate and cathodic potentials. In some samples at anodic potentials, both IGA and SCC were observed. In fact, the anodic potential limit of IGA overlapped with the lower limit of the SCC region.

POLARIZATION CURVES IN CAUSTIC - Fig. 5 shows the polarization curves of Alloy 600 in 10% and 0.1% NaOH solutions at 300 C at a scan rate of 20 mV/min. Both curves show activation controlled regions, and active-passive transitions followed by regions of passivity. The values of the critical current density for passivation and the passive current density at the higher concentration are larger by at least an order magnitude than those at the lower concentrations. However, the potential for active-passive transition appears to be rather independent of the concentration.

C-RINGS IN SIMULATED PRIMARY WATER - Six different C-rings were held in the simulated primary water within the potential range of -300 to +430 mV (vs. platinum which was used as a reference electrode), using the Seys and Van Haute potential gradient technique described earlier. The specimens were held at 340 C for 12 days and later (in a new run) at 315 C for 25 days. Specimens at -300 mV (see Fig. 6) and at +150 mV suffered SCC, with an average propagation rate of about 0.03 μm/h. The one at 0 mV had minor intergranular penetration and the other three (+430, +300 and -160 mV respectively) were not attacked. The open circuit potential of Alloy 600 with respect to platinum was 0 mV in this environment. Thus, it appears that SCC in this environment may occur both in the anodic and the cathodic potentials. Although the cracks in Fig. 6 appear to be very shallow, the crack propagation rate is consistent with what is generally observed in this type of system. Thus, freely corroding reverse U-bends give a propagation rate of only 0.01 μm/h in the 325-330 C range in pure or primary water (4). A somewhat

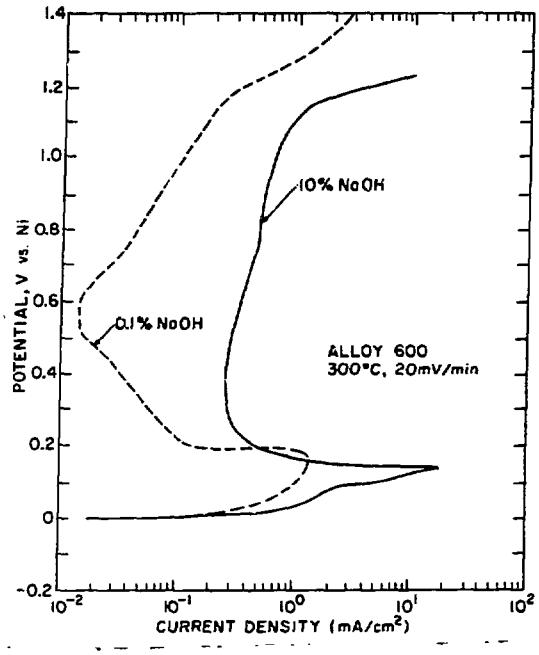

Fig. 5 - Polarization curves for Alloy 600 in 10% and 0.1% NaOH at 300 C.

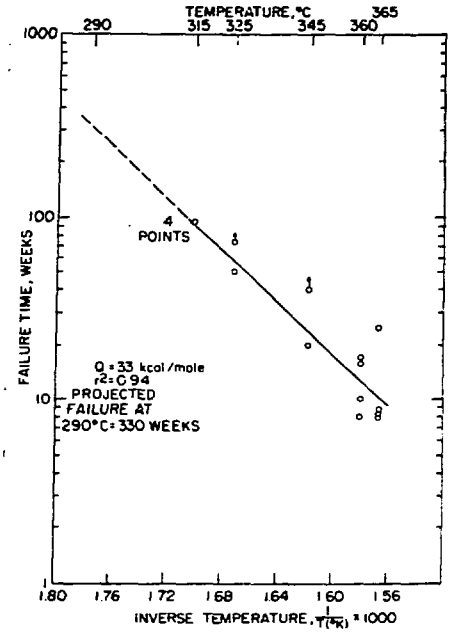

Fig. 7 - SCC of Alloy 600 U-bends (0.01% C) in deaerated pure water.

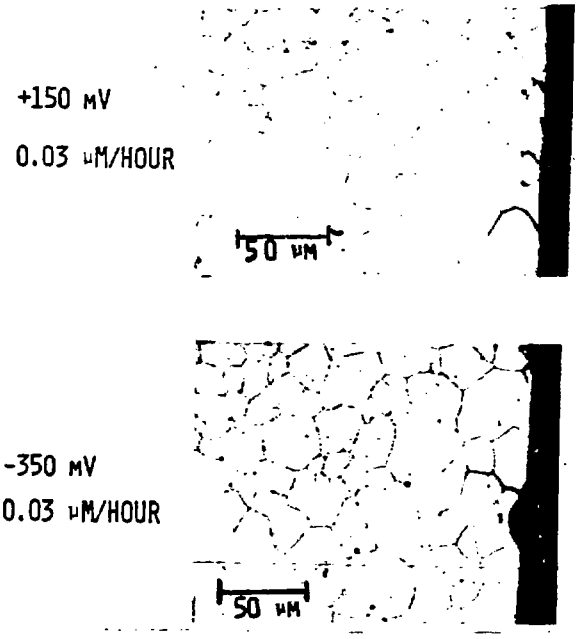

Fig. 6 - SCC of C-rings at +150 and -300 mV vs. platinum in high temperature simulated primary water.

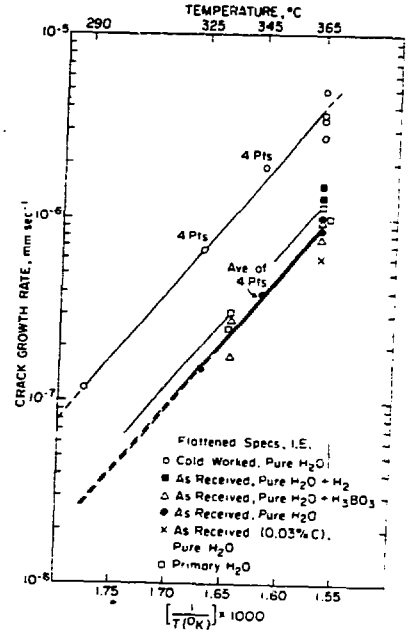

Fig. 8 - Environmentals effects in slow strain rate tests on Alloy 600, 0.01% C and 0.03% C.

higher propagation rate in Fig. 6 suggests that applied potential accelerates the rate.

U-BENDS IN HIGH TEMPERATURE WATER - Fig. 7 shows results of U-bend tests in pure deaerated water, giving an activation energy of 33 Kcal/mole. Although the U-bend calculations are not very precise, an average crack growth rate of 6×10^{-7} mm sec^{-1} is obtained at 365 C. This compares to a value of about 8×10^{-7} mm sec^{-1} in slow strain rate tests at 365 C described in the following section. It should be kept in mind that U-bend tests do not allow an accurate estimate of stress relief during exposure, which may contribute to longer SCC times in U-bends.

Hydrogen accelerated the SCC of U-bends in pure water. In an exposure of nine different heats to pure H_2O and $H_2O + H_2$ at 365 C, only 2% failure occurred in 12 weeks in the former environment compared to 83% failures in the latter.

SLOW STRAIN RATE TESTS IN HIGH TEMPERATURE WATER - Slow strain rate test data show that this method does not fully eliminate the initiation stage of SCC, i.e., cracks do not start when the test begins, nor, in fact at the onset of plastic deformation; it takes a finite time (after yielding) for SCC to develop. Initiation times are however, much shorter than for U-bends, and vary with temperature. Fig. 8 shows a family of straight line Arrhenius plots of constant extension rate testing data, obtained at strain rates of about 2 to 3×10^{-8} sec^{-1}. A heat of 0.01% C was used for most of these data, although another heat of low carbon and one of 0.05% C agree in general with the slopes given here, and an activation energy of about 33 Kcal/mole can be calculated for material as cold worked, or aged (365 C), or mill annealed, suggesting that these treatments do not affect the crack propagation mechanism. We have used a method of extrapolating plots of crack length vs. strain (down to zero crack length) in order to determine the point at which SCC starts and calculated the propagation rate accordingly.

Cold work increases SCC velocity as can be seen from the results for flattened specimens in Fig. 8. Hydrogen added to the test medium also increases the propagation rate, as shown in Fig. 8, at least in the case of the as-received material where we observe the greatest spread between the various curves obtained from different environments. Opposed to this hydrogen effect there appears to be a lowering in the crack velocities due to an increase in pH such as would result from the addition of lithium hydroxide to the test medium. As a result it appears that simulated primary water is not substantially different from pure water in this particular test procedure.

MECHANISTIC ASPECTS OF INTERGRANULAR FAILURES-

1. Caustic Environment - The onset of rapid SCC in caustic generally coincides with the potential corresponding to the active-passive transition, and at potentials where the passivity is well established (approximately 300 mV), crack growth rate falls sharply (Fig. 2). This suggests a film-rupture type model for the SCC process (12,13). Thus, cracking proceeds due to the rupture of the film caused by transient creep followed by anodic dissolution along the grain boundary and subsequent repassivation. The grain boundary and a narrow area adjacent to it may be anodic to the bulk material or otherwise more favorable for enhanced dissolution. First, strain is likely to be greater near the grain boundary which may also be the site of numerous dislocation pile-ups. Second, the compostion of the grain boundary may differ from the bulk composition. Third, the film composition on the sample above the grain boundary may differ from that on the bulk. Fig. 9 shows the nature of attack on an Alloy 600 coupon after an exposure for 10 days in 10% NaOH + 1% Na_2SO_4 solution at 315 C at a potential of 150 mV anodic to the corrosion potential. It is evident from the grain boundary grooving that grain boundaries are preferred sites for the intergranular failures. The sulfate was added in this test as an impurity and does not appear to significantly influence the SCC or IGA mechanisms.

The surface freshly created by rapid straining of the film-covered surface into the plastic region provides information regarding the maximum crack propagation rate (14). Therefore, the steady and transient currents from an Alloy 600 wire specimen held in the potential region of 150 to 250 mV in 10% NaOH + 0.1% Na_2CO_3 at 300 C were recorded, as shown schematically in Fig. 10. The current measured during straining, i_y, is given by (9)

$$i_y = (i_s \times A_s) + (i_b \times A_b) \qquad (1)$$

where,

i_s = current density on the filmed metal

A_s = fraction of specimen area covered by the film

i_b = current density on the bare metal

A_b = fraction of specimen with bare metal

It is assumed that i_s remains constant during straining and the transient current comes from the dissolution of the newly exposed bare metal where the film breaks. The amount of fresh surface produced due to straining is (14):

$$\% \text{ Bare surface} = 100 \left[(L/L_o)^{\frac{1}{2}} - 1 \right] \qquad (2)$$

where L_o is the initial length and L is the length at any time during straining. For small linear strains, equation (2) reduces to (9):

$$\% \text{ Bare surface} \simeq 1/2(\% \text{ strain}) \qquad (3)$$

The following typical current density values were obtained in our test:

$i_s = 1.0$ mA/cm^2

$i_b = 20.9$ mA/cm^2 at approximately 200 mV.

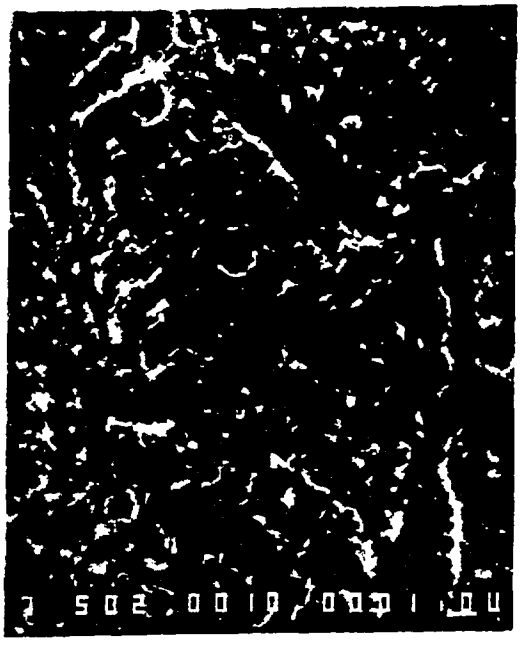

Fig. 9 - Nature of surface attack on an Alloy 600 coupon after exposure for 10 days in 10% NaOH + 1% Na_2SO_4 solution at 315 C at +150 mV vs. Ni, showing grain boundary grooving.

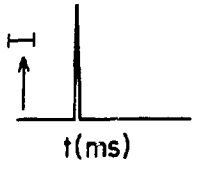

RAPID STRAINING

E = 150 mV

$$V = \frac{i_b \cdot E}{F \cdot d} = 26.6\,\mu m/h = 7.4\ nm/s$$

i_b BASED ON BUBAR & VERMILYEA

Fig. 10 - Determination of crack propagation rate from a straining electrode in 10% NaOH + 0.1% Na_2CO_3 at 300 C at +200 mV vs. nickel.

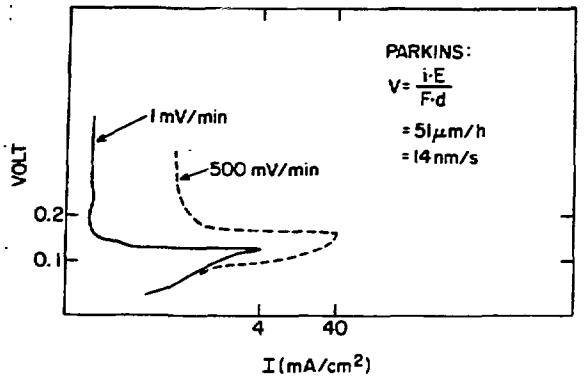

Fig. 11 - Polarization curves of Alloy 600 in 10% NaOH at 300 C at a slow and a fast scan rate, and the determination of crack propagation rate from the latter. Potential was measured against a Ni reference electrode.

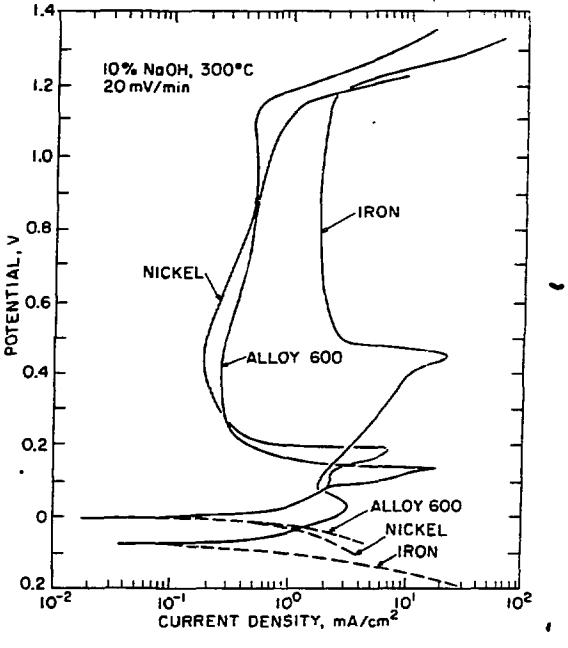

Fig. 12 - Polarization curves for Fe, Ni and Alloy 600 in 10% NaOH at 20 mV/min.

The maximum CPR, V_m, is related to the maximum i_b value through the equation (14):

$$V_m = (i_b.E)/(F.d) \qquad (4)$$

where E, is the mean equivalent weight for the metal, d its density and F the Faraday constant. Using an E of 29 g/eq, and d of 8.5 g/cm^3 for Alloy 600 (9), one obtains the maximum CPR, V_m = 26.6 μm/h.

Based on rapid polarization scan in the above environment (Fig. 11) and applying the Faradaic dissolution model, i.e., Eq. (4), one obtains a propagation rate of 51 μm/h. Some recent slow strain rate tests (15) on Alloy 600 in 10% NaOH at 316 C and an applied potential of 150 mV give an average crack propagation rate of 15.3 μm/h which includes the initiation time. If the approximate initiation time is excluded, a somewhat higher value of 18.5 μm/h is obtained. Thus, the experiental value is very similar to the one calculated above on the basis of the film rupture model. The value derived from rapid polarization scan appears to be rather high, where-as the C-rings give appreciably lower values (Fig. 2), presumably because of a large percent-age of the testing time involved in crack initiation.

In our tests with C-rings under potential control, no SCC was observed at 0 mV in 10-12 days. However, there are numerous data in literature showing SCC of C-rings or U-bends after exposure for several months in high temperature caustic under freely corroding conditions (1,2). This apparent discrepancy may be resolved by any or all of the following arguments: (1) the corrosion potential of the specimen gradually drifts anodiccally and eventually reaches a potential conducive to film formation, leading to SCC. (2) the initial phase of dissolution of the metal is followed by a precipitation reaction of the noble component of the alloy, i.e., nickel, giving a pseduo-passive layer, which when ruptured will facilitate localized dissolution and hence SCC. EDX analysis of one of our coupons corroded freely in high temperature caustic gave a pure nickel spectra perhaps in line with the above argument. (3) Another attractive possibility is the gradual dealloying of the alloy due to preferential dissolution of iron in high temperature caustic. The polarization curves for iron, nickel and Inconel in 10% NaOH at 300 C (Fig. 12) show clearly that at 0 mV, i.e., the E_{corr} of Alloy 600, iron corrodes at least two orders of magnitude faster than nickel and Alloy 600. Tests with chromium are currently underway. The dealloying is manifested initially as an IGA type of attack as observed by us, but may eventually lead to SCC. According to this model, IGA is simply a precursor to SCC.

Fig. 13 shows the nature of surface attack on Alloy 600 coupon held for 10 days at 25 to 45 mV in 10% NaOH + 1% Na_2SO_4 at 315 C. The surface is generally etched, but some areas are completely covered with a dark film. In this potential region where the coupons are partially covered with a film, the anodic potential limit of IGA overlaps tne lower limit of the SCC region. This observation may allow a tentative assumption that stress is possibly not an important factor in the initiation of IGA in this potential region. Indeed, in this overlapping region, as soon as a reasonable stress is applied, it probably modifies the IGA morphology into a SCC morphology. Fig. 3, however, shows that IGA occurs at potentials both anodic and cathodic to the corrosion potential. It is clear that increasing anodic potential tends to accelerate the IGA rate, perhaps related to the way that anodic potential causes increased dissolution in the activation controlled region of the polarization curve (Fig. 5). Thus, IGA may be related to the overall uniform corrosion rate in a complex way.

The mechanism governing the IGA at cathodic potentials (Fig. 3) is not well understood. One explanation is that in the cathodic potential region of interest, the dealloying process is perhaps still operative. In this potential zone, the dinickelite and dihypoferrite ions are the stable species, formed by the following reactions respectively (16):

$$Ni + 2H_2O = HNiO_2^- + 3H^+ + 2e \qquad (5)$$

$$Fe + 2H_2O = HFeO_2^- + 3H^+ + 2e \qquad (6)$$

Both of these ions have extended stability in the regions cathodic to the corrosion potential of Alloy 600 and the stability regions expand with increasing temperature. Also, the possible role of an hydrogen assisted attack at cathodic potentials should not be ignored.

2. High Temperature Water - SCC in high temperature water is strongly temperature dependent, is accelerated by hydrogen and cold working, and appears to occur at potentials both anodic and cathodic to the corrosion potential. Fig. 5 shows that the alloy exhibits an active-passive behavior even in 0.1% NaOH. If one assumes that the mechanism of SCC in very dilute caustic and water at high temperature is very similar (17), then it may be argued that the SCC in high temperature water at anodic potentials is governed by a film-rupture mechanism perhaps very similar to the one that governs the SCC in caustic. Currently, SCC tests are underway in very dilute caustic solution. The crack propagation rates from these tests will provide more knowledge regarding the relationship between SCC in high temperature water and dilute caustic solutions. Note that in the C-ring tests (in Fig. 6), the specimens at 300 and 430 mV did not crack, perhaps because of the establishment of a very stable passivity at these potentials. This is in line with the absence of SCC in caustic at beyond 300 mV (Fig. 2).

In high temperature water, significant cracking is observed in U-bends and slow strain rate tests under freely corroding conditions (Fig. 7 and 8). Alloy 600 coupons exposed to high temperature water show evidence of an oxide film on the surface. A piece of Alloy 600 specimen cut directly from a tube was immersed in deaerated, pure water at 365 C for about two weeks. After withdrawal, the specimen was shadowed with

Fig. 13 - Nature of surface attack on an Alloy 600 coupon after an exposure for 10 days in 10% NaOH + 1% Na_2SO_4 solution at 315 C at a potential of +25 to 45 mV vs. Ni.

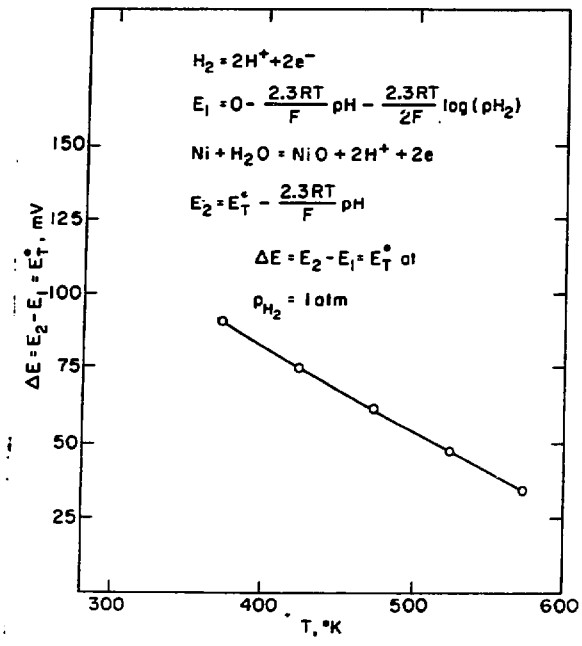

Fig. 15 - Relationship between temperature and the equilibrium potential for NiO formation from freshly generated nickel in an aqueous environment with a hydrogen pressure of 1 atmosphere.

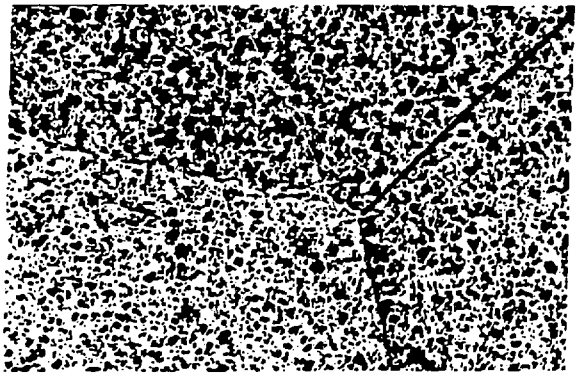

Fig. 14 - TEM micrograph of oxide film grown on Alloy 600 coupon in deaerated pure water at 365 C for approximately two weeks.

Fig. 16 - Replica factographs of Alloy 600 specimen cracked in a slow strain rate test at 365 C, showing an area covered with oxide with parallel rupture markings.

carbon (to avoid shattering) and the surface film was stripped using a 10% bromine-methanol solution. The film was mounted on a copper grid and analyzed on a JEOL 100 electron microscope. Fig. 14 shows a typical micrograph of the film consisting of several components some of which appeared to have regular crystallographic patterns and gave well defined diffraction patterns. Note in Fig. 14 that the growth of the film appears to be different in different grains, perhaps influenced by orientation. It is clear that the film retains the grain boundaries of the substrate and therefore fracture might be expected to follow the boundary, a plane of weakness especially in mechanically weak substances. The oxide film is rich in Ni (as observed in EDX) and is probably formed by oxidation of nickel to its oxide according to the reaction:

$$Ni + H_2O = NiO + 2H^+ + 2e \qquad (7)$$

The equilibrium potential for NiO formation (16) approaches the hydrogen redox potential as the temperature is increased, as shown in Fig. 15. At present, we do not have any thermodynamic data beyond 300 C. It is possible that at 365 C, NiO forms at the corrosion potential of Alloy 600 which is equal to the hydrogen redox potential at a partial pressure of hydrogen equal to one atmosphere (as in primary water) (18). The increased susceptibility to SCC at around 365 C may at least be partially explained on the basis of the ease of oxide formation and its subsequent rupture at this temperature. Fig. 16 illustrates a replica fractograph of an Alloy 600 sample cracked in pure water at 365 C, showing an area covered with oxide with parallel rupture markings which perhaps resulted from the strain induced in the film. In a stressed sample, the creep in the metal ahead of the film introduces increasing elastic strain in a mechanically weak film, eventually leading to fracture. The crack is arrested by plastic deformation when it enters the substrate and the environment again will have direct access to the metal, leading to fresh oxide film formation. The process is repeated leading to discontinuous crack propagation. In this model, it is assumed that the creep rate at the crack tip would be greatly influenced by the magnitude of the local stress. Also, the activation energies for region I and II (in a crack velocity (V) vs. stress intensity (K) curve) of crack growth would generally correspond to those for transient creep and a mass-transport-limited anodic dissolution process, respectively (13).

Both U-bends and slow strain rate tests in pure water (Figs. 7 and 8) give a relatively high activation energy of 33 Kcal/mole compared to the SCC of numerous other alloys in various other media (19-21). Speidel (19) and Blackburn et al. (20) have discussed the activation energy question for SCC in various alloy-environments. For many Al, Mg, and Ti alloys in aqueous halide media, organic solvents, and molten salts, activation energies near 4 Kcal/mole have been measured in stage II crack growth (19). For region I, however, the activation energies are about 27 to 28 Kcal/mole for Ti, Al alloys and glass (19,20). Ohtani and Hayashi (21) report an activation energy of 20-23 Kcal/mole for stainless steel - $MgCl_2$ system. For Al alloys, Speidel (19) gives the SCC velocity in stage II region as:

$$V = C_2 \exp\left[(-Q/RT)\right] \qquad (8)$$

where Q is the apparent activation energy, C_2 is a constant, R and T have usual meanings. For stage I, however, the above equation is modified to:

$$V = C_3 \exp\left(-Q + C_4 K_I\right)/RT \qquad (9)$$

where C_3, C_4 are constants, Q is the activation energy and K_I is the crack tip stress intensity. The high activation energy observed in our system thus implies that the SCC in high temperature water is influenced primarily by mechanical processes involving transient creep in the stage I region.

The cracking in simulated primary water at -300 mV (Fig. 6) suggests the possibility of a hydrogen assisted mechanism. This is further reinforced by the fact that cold working and the presence of hydrogen accelerate the rate of crack propagation.

In summary, Alloy 600 suffers rapid SCC in caustic in the anodic potential range of 150 to 200 mV, with marked reduction of the propagation rate at higher and lower potentials. This SCC seems to be governed by a film-rupture mechanism. At lower potentials, IGA and some SCC are observed and the two are often overlapped. A dealloying mechanism may be involved in these processes. Increasing anodic potential tends to accelerate IGA, perhaps related to the way that anodic potential causes increased dissolution in the activation controlled region of the polarization curve in caustic. IGA may be a precursor to SCC in that both involve some kind of grain boundary corrosion, with SCC having an additional mechanical factor related to the strain rate due to creep processes. SCC in primary and pure water occurs at anodic potentials (150 mV) controlled by a film-rupture mechanism. No SCC is observed at 300 mV and beyond because of the occurrence of stable passivity. Cracking at cathodic potentials is governed perhaps by a hydrogen assisted mechanism. In certain potential regimes (say, the corrosion potential), the two mechanisms may overlap.

ACKNOWLEDGEMENT

The work in the caustic and high temperature water environments were supported by the Electric Power Research Institute and U.S. Nuclear Regulatory Commission respectively. Discussion with A.R. McIlree, J.P.N. Paine and J.R. Weeks are acknowledged. Thanks are due to C. Schnepf and T. Roberts for technical assistance.

REFERENCES

1. Green S.J. and Paine, J.P.N., Nuclear Technology, 55, 10 (1981).

2. Airey, G.P., and Pement, F.W., Corrosion, 39, 46 (1983).

3. Bulischeck, T.S. and van Rooyen, D., Nuclear Technology, 55, 383 (1981).

4. Bandy, R. and van Rooyen, D., Corrosion, 40, 425 (1984).

5. Theus, G.J. and Cels, J.R., Stress Corrosion Cracking - The Slow Strain - Rate Technique, ASTM STP 665, G.M. Ugiansky and J.H. Payer, Eds., ASTM pp. 81-96 (1979).

6. Pessall, N., Corrosion Science, 20, 225 (1980).

7. Berge, Fh., Donati, J.R., Prieux, B. and Villard, D., Corrosion, 33, 425 (1977).

8. Seys, A.A. and Van Haute, A.A., Corrosion, 29, 329 (1973).

9. Park, Y.S., Galvele, J.R., Agrawal, A.K. and Staehle, R.W., Corrosion, 34, 413 (1978).

10. Bandy, R. and Van Rooyen, D., Corrosion, 40, 281 (1984).

11. Sedriks, A.J., Floreen, S. and McIlree, A.R., Corrosion, 32, 157 (1976).

12. Vermilyea, D.A., "A Film Rupture Model for Stress Corrosion Cracking," in Stress Corrosion Cracking and Hydrogen Embrittlement of Iron Base Alloys, p. 208, Firminy, France, June 12-16 (1973).

13. Pugh, E.N., "A Film Rupture Model for Stress Corrosion Cracking," in Stress Corrosion and Hydrogen Embrittlement of Iron Base Alloys, p. 37, Firminy, France, June 12-16 (1973).

14. Bubar, S.F. and Vermilyea, D.A., J. Electrochem. Soc., 113, 892 (1966).

15. Crum, J., Paper No. 178, Corrosion '84, New Orleans, April 2-6 (1984).

16. Cowan, R.L. and Staehle, R.W., J. Electrochem. Soc., 118, 557 (1971).

17. Berge, Fh., and Donati, J.R., Nuclear Technology, 55, 88 (1981).

18. Cowan, R.L. and Tedmon, C.S., "Advance in Corrosion Science and Technology," Vol. 3, ed. M.G. Fontana and R.W. Staehle, Plenum Press, New York, p. 293 (1973).

19. Speidel, M.O., "The Theory of Stress Corrosion Cracking in Alloys," ed. J.C. Scully, NATO, p. 289 (1971).

20. Blackburn, M.J., Feeny, J.A. and Beck, T.R., "Advances in Corrosion Science and Technology," Vol. 3, eds. M.G. Fontana and R.W. Staehle, Plenum Press, New York, p. 148 (1973).

21. Ohtani, N. and Hayashi, Y., "Passivity and its Breakdown on Iron and Iron Base Alloys," USA-Japan Seminar, eds. R.W. Staehle and H. Okada, p. 169 (1976).